Properties of a Parameterization of Radon Projection by the Reconstruction on Circular Disk

O. Tischenko[a], A. Schegerer[a], Y. Xu[b] , C. Hoeschen[a]
[a]Helmholtz Zentrum Muenchen, German Research Center for Environmental Health, Ingolstaedter Landstrasse 1, D-85764 Neuherberg, Germany
[b]Dept. of Mathematics, University of Oregon, Eugene OR 97403-1222, USA

ABSTRACT

An angular parameterization of parallel Radon projections referred to in this paper as ψ-parameterization is discussed in relevance to the efficiency of reconstruction from fan data. The fact that the ψ-parameterization coincides with the equiangular fan beam parameterization allows us to develop a simple and efficient approach useful for the reconstruction from fan data. Within this approach parallel projections are approximated by groups of semi-parallel rays. The reconstruction is carried out directly, i.e. without any modification of original data, at the speed which is comparable or even higher than that of the parallel Filtered Back Projection (FBP) algorithm.

Keywords: CT, Tomography, Reconstruction, fan beam

1. INTRODUCTION

The most common algorithm used for the reconstruction of clinical data is Filtered Back Projection (FBP) (see e.g [1,2]). Parallel beam FBP is the algorithm for which the input data are supposed to be measured over sets of equi-spaced parallel lines that intersect the object. The weighted FBP, or fan beam FBP, can be used for the reconstruction of fan data, that is, data measured over ray sets generating fans diverging from a point source. Because of the lower computational cost and higher stability, parallel beam FBP is often preferable. However, in order to apply the parallel beam FBP for fan data, these have to be resampled to equi-spaced parallel data. In this case one faces the problem of resampling from a non-uniform grid to a uniform one. Indeed, samples of fan data generate a non-uniform grid in parallel beam coordinates, and this non-uniformity is even higher when the fan angle becomes larger. As a consequence, the resampling step is connected with the risk of loosing the information contained in the original data. Projections generated by parallel rays intersecting points, which are uniformly distributed on the boundary of disk, represent an example of data which can be resampled to fan data and vice versa without loss of information. Projections of such geometry are referred in this paper to as ψ-projections, and the corresponding parameterization as ψ-parameterization. The algorithm is required that allows to reconstruct from ψ-projections.

One of the specific requirements for the reconstruction algorithm OPED (Orthogonal Polynomial Expansion on Disk) is that Radon projections have to be ψ-projections. This means that fan data can be resampled to data required by OPED via some loss-free interpolation. In fact, we show that fan data can be used with OPED directly, without any modification. The image reconstructed within this approach is a very close approximation of the image reconstructed from exact ψ-projections. In this sense, OPED provides an excellent trade-off between the speed and the accuracy of the reconstruction from fan beam data. This algorithm was introduced in [3]. In [4] it was shown that it is stable, provides high resolution images, and has a small global error. The numerical efficiency of the algorithm was studied in [5,6]. There it was shown that the reconstruction made with OPED can be implemented with a number of operations of the same order as with parallel FBP [5], or even faster [6].

In section 2 we recall the main formula of OPED and present the method of reconstruction from fan data. The results of this method are presented in section 3 and discussed in section 4.

Medical Imaging 2010: Physics of Medical Imaging, edited by Ehsan Samei, Norbert J. Pelc,
Proc. of SPIE Vol. 7622, 76222F · © 2010 SPIE · CCC code: 1605-7422/10/$18 · doi: 10.1117/12.845252

2. MATERIALS AND METHODS

2.1 The OPED Algorithm

Let *B*, $B := \{(x,y), x^2 + y^2 \le 1\}$ be the unit disk and let $p(\phi,\cdot)$ be ϕ-projection of function *f* supported on *B*,

$$p(\phi,t) = \int_{B \cap L(\phi_v,t)} f(x,y)dxdy\,,$$

where $L(\phi,t) := \{\, x\cos\phi + y\sin\phi = t \,\}$ is the line intersecting the disk. Let p_v denote ϕ_v-projection of *f*, $t' = x\cos\phi_v + y\sin\phi_v$ and $\phi_v = v\pi/n$, $v = 0,\ldots,n-1$. OPED is based on the formula

$$A_n f(x,y) = \frac{1}{n}\sum_{v=0}^{n-1}\sum_{k=0}^{m-1}(k+1)U_k(t')\frac{1}{\pi}\int_{-1}^{1} p_v(t)U_k(t)dt \tag{1}$$

(see [3]), where $U_k(t)$ is a Chebyshev polynomial of second kind (for definitions see e.g.[7]), and $A_n f$ is the approximating polynomial, which is optimal in the sense that among all polynomials P_n of degree $\le n$, the norm

$$\|P_n - f\|_2 = \left(\int_D (P_n(x,y) - f(x,y))^2 dxdy\right)^{1/2} \tag{2}$$

is minimized when $P_n = A_n f$. Changing in (1) variable *t* to $\psi = \arccos t$ and replacing the integral by a Gaussian sum over points ψ_j, $0 \le j < m$ uniformly distributed over *π*, one obtains the following approximation

$$A_n f(x,y) \approx \frac{1}{n}\sum_{v=0}^{m-1}\frac{1}{m}\sum_{j=0}^{m-1} p_v(\psi_j)\Phi_m(\psi_j,\psi'),\ \cos\psi' = x\cos\phi_v + y\sin\phi_v\,, \tag{3}$$

$$\Phi_m(\psi,\psi') = \sum_{k=0}^{m-1}(k+1)\sin(k+1)\psi\,\frac{\sin(k+1)\psi'}{\sin\psi'}\,,$$

which is exact if p_v is a trigonometric polynomial of degree up to 2*m*. For kernel Φ_m the following compact representation is valid:

$$\Phi_m(\psi,\psi') = (h_m(\psi'-\psi) - h_m(\psi'+\psi))\sin^{-1}\psi' \tag{4}$$

$$h_m(\psi) = \frac{1}{4}\left(m\sin(2m+1)\frac{\psi}{2}\Big/\sin\frac{\psi}{2} - \sin^2 m\frac{\psi}{2}\Big/\sin^2\frac{\psi}{2}\right)$$

(see Appendix). The formula (3) can be evaluated fast in two steps: 1) transformation of projections

$$\hat{p}_{v,k} = \frac{1}{m}\sum_{j=0}^{m-1} p_v(\psi_j)\Phi_m(\psi_j,\psi_k) \tag{5}$$

followed by a back projection

$$A_n f(x,y) = \frac{1}{n}\sum_{v=0}^{n-1}\hat{p}_v(\psi'),\ \cos\psi' = x\cos\phi_v + y\sin\phi_v\,, \tag{6}$$

where $\hat{p}_v(\psi')$ can be approximated e.g. via linear interpolation between entries of matrix $\hat{p}$ defined in (5). As it was shown in [5], the number of operations required for the evaluation of (3) within this approach is of the same order as that used for the reconstruction with the parallel beam FBP. The number of operations can even be reduced significantly for special types of evaluation grid (see below and [6]).

As it follows from (4), the transformation of projections consists of two convolutions with kernel *h* and scaling with factor $\sin^{-1}\psi'$. In fact, the transformation of projections is not as time consuming as the back projection, which takes more than 90% of the whole computing time. Therefore, the gain obtained via applying fast Fourier methods for the implementation of convolution is not essential. Moreover, in many cases it is more convenient to carry out the direct calculation expressed by (5).

Especially for $\psi_k = \pi k / m$ the kernel Φ_m takes a very simple form:

$$\Phi_m(\psi_j, \psi_k) = \begin{cases} \dfrac{1}{4}\dfrac{m}{\sin\psi_k}, & \text{if } k = j \\ -\dfrac{\sin\psi_j}{m(\cos\psi_j - \cos\psi_k)^2}, & \text{if } k + j \text{ is odd} \\ 0, & \text{otherwise} \end{cases} \tag{7}$$

A profile of the kernel (5) by fixed *k* is shown in Fig. 1

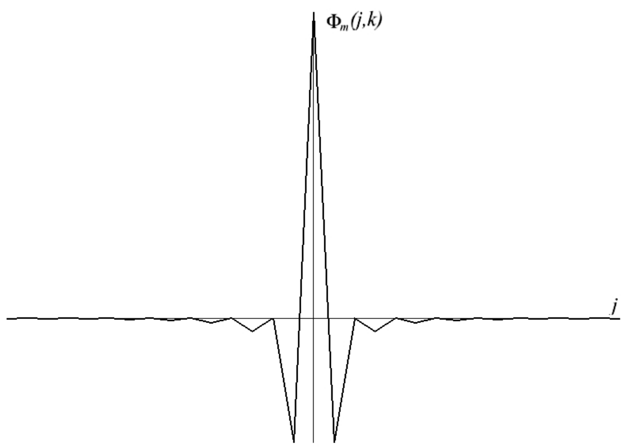

Figure 1. A profile of the kernel Φ_m by fixed *k*.

As it can be seen in Fig. 1, the profile of the kernel Φ_m by fixed *k* is very similar to the impulse response of the Ramp filter. However, as it follows from (7), the kernel $\Phi_m(\cdot, k)$ is not shift invariant. It is slightly asymmetric and scaled according to a local distance between rays within the projection.

2.2 Properties of the ψ-parameterization

The practical impact of ψ-parameterization reveals itself first of all in that parallel data distributed uniformly in terms of parameter ψ can be measured directly in the fast non-stop mode [8-11]. The computing efficiency can be significantly enhanced for data collected over rays distributed accordingly. Finally, properties of ψ-parameterization can be used for developing a simple approach for the reconstruction from fan data.

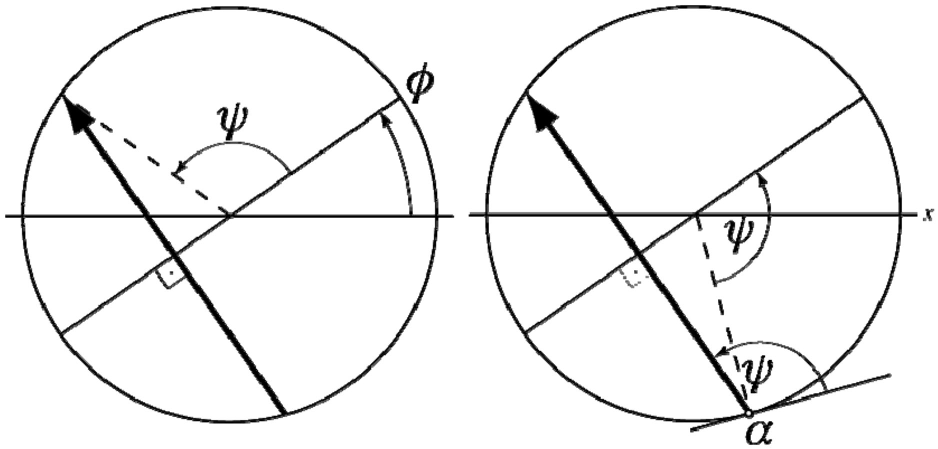

Figure 2: The ray (thick oriented line) characterized with angle parameters (φ, ψ)

In Fig. 2, left, the ray emitted from the boundary of the disk and characterized by parameter ψ is depicted. The angle under which this ray is emitted from point source α (see Fig. 2, right) is again ψ. Hence, the ψ-distribution of rays within parallel projection coincides with the angular distribution of rays within a fan. The following transformation between parallel beam coordinates (φ,ψ) and fan beam coordinates (α,ψ) is valid:

$$\phi = \alpha + \psi \ . \tag{8}$$

2.3.1 Computing efficiency

The effect of the ψ-parameterization on computing efficiency can be demonstrated with the following example. Let data be associated with sets of parallel rays (ϕ_v, ψ_j),

$$\phi_v = \frac{2\pi v}{n}, \psi_j = \left(\frac{1}{2} + j\right)\frac{\pi}{n}, 0 \le v, j < n. \tag{9}$$

Equivalently, this data can be associated with fans of rays (α_v, ψ_j)

$$\alpha_v = \frac{2\pi v}{n}, \psi_j = \left(\frac{1}{2} + j\right)\frac{\pi}{n}, 0 \le v, j < n \ . \tag{10}$$

On the left hand side of Fig. 3, the fan of rays is shown for the case n=9. For each ray of this fan there is a point in the unit disk where the ray intersects the circle of radius ½ (white dot in Fig. 3, left). A set consisting of these points and those lying between of them (black dots in Fig. 3, left) is referred to as S_0. Let S_j be the set of points obtained from S_0 via rotation of the latter at the angle π/n around the center of the disk. A set $\bigcup_{0 \le j < 2n} S_j$ generates the grid on the disk (right in Fig. 3) that can be used as a primary evaluation grid.

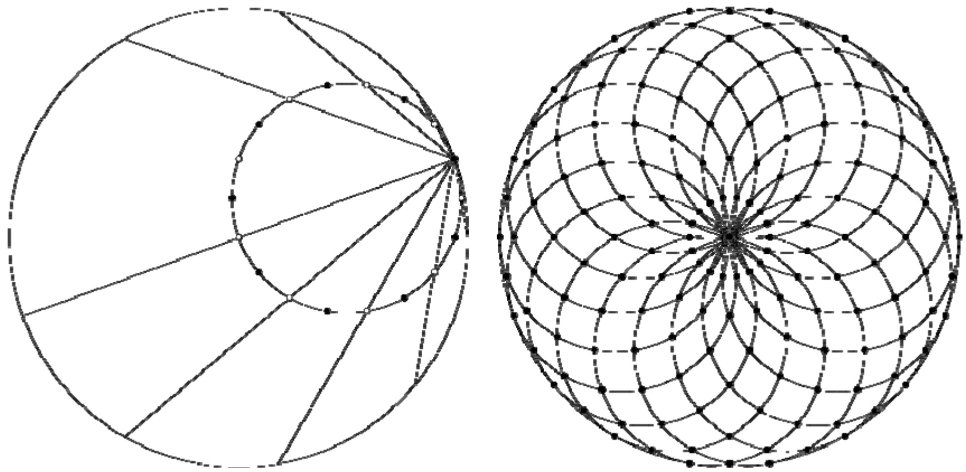

Figure 3. left: A fan of rays and the points associated with them ; right: primary evaluation grid

This grid has the following remarkable properties: 1) the distribution and the number of grid points provides conditions for recover a unique polynomial of order up to $2n$, 2) it is circularly symmetric and 3) the distance between its neighboring points lying on the same ½-circle is constant (see the figure). Using the symmetry of this grid, the number of operations required for the computation of interpolating weights during the back projection (see section 2) can be reduced drastically. The fact that a predefined half of grid point is intersected by reays accelerated the process of reconstruction even more. In order to represent the reconstruction, the result of primary evaluation has to be resampled to the Cartesian grid. The property 3 can be used for designing an efficient resampling algorithm based on the bi-linear interpolation.

2.3.2 Reconstruction from fan data

In general, using the fan-parallel transformation expressed by equation (8), any fan data can be represented on (φ,ψ)-plane as shown on the right hand side of Fig. 4.

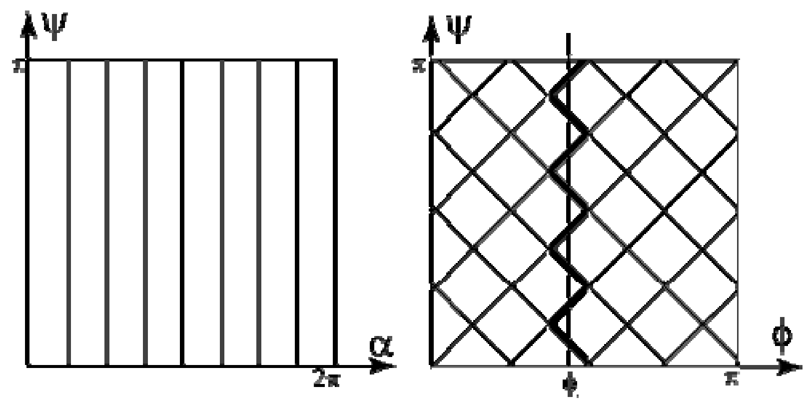

Figure 4. Two different representation of the same fan data. Fans generate lines α = *const* in fan beam coordinates (vertical lines, left), and lines $\varphi = \alpha + \psi$ in parallel beam coordinates (slope lines, right)

The whole data set can be resorted into n groups related to non-overlapped segments $[\phi_v - \Delta\phi/2, \phi_v + \Delta\phi/2]$, $0 \le v < n$, of the φ-axis. One of these groups is distinguished on the right of Fig. 4 (thick broken line). Data samples of one such group constitute an approximation of the ψ-projection at a given orientation (expressed e.g. with the projection angle ϕ_v in Fig. 4.). More specifically, assume that fan data have been measured over rays (α_v, ψ_j),

$$\alpha_v = \frac{2\pi v}{n} = v\Delta\alpha,\ 0 \le v < n, \tag{11}$$

$$\psi_j = \left(j + \frac{1}{2}\right)\frac{\pi}{m} = \left(j + \frac{1}{2}\right)\Delta\psi,\ 0 \le j < m \tag{12}$$

under the condition that $\Delta\alpha = 2r\Delta\psi$, where $r \ge 1$. If $r = 1$, then $m = n$ and the set of all rays is equivalently represented as a set of n ψ-projections each containing n rays distributed according to (12). If r is integer and $r > 1$, then rays are organized as a set of n groups with m rays in each of them. The ψ-distribution of rays within these groups is expressed with (12), but rays are not parallel but semi-parallel. The spatial configuration of rays within the semi-parallel group for $n = 8$ and $r = 3$ is depicted in Fig. 5.

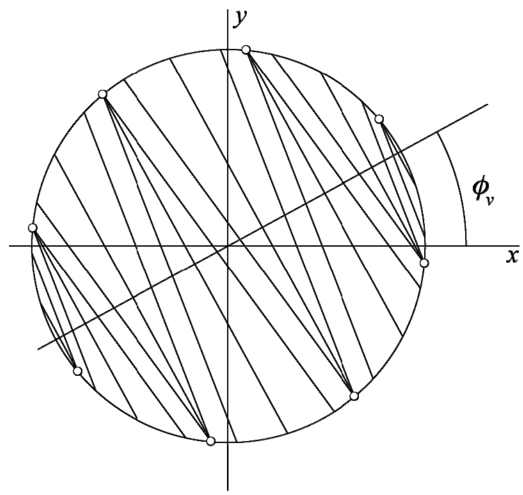

Figure 5. A group of semi-parallel rays associated with projection angle φ for r = 3.

During the reconstruction, semi-parallel groups are treated as if they were ψ-projections.

Note that true orientations of rays in the semi-parallel group are $\phi_{v,j}$, $\phi_{v,j} = \phi_v \pm \left(\frac{r-1}{2} - j\right)\Delta\psi$. That is, the deviation $\delta\phi_j = \left|\phi_v - \phi_{v,j}\right|$ from the ideal orientation ϕ_v for any ray within the semi-parallel group is $\delta\phi_j = \left|\frac{r-1}{2} - j\right|\Delta\psi$, $0 \le j < r$, and consequently the maximum deviation is $\delta\phi_j = \frac{r-1}{2}\Delta\psi$.

3. RESULTS

In Fig. 6 there are two reconstructions of the abdominal phantom. Two data sets have been simulated using a Monte Carlo approach, fan data and parallel data. The phantom was supposed to be situated in the middle of the unit disk, namely, inside of a circle with radius 1/3, while the x-ray source is positioned on the boundary of the disk. In both cases detectors of the same resolution have been used.

Fan data were simulated in the "stop-and-start" mode, i.e. projections for each view were generated by fixed positions of the x-ray source. The number of views was set to n = 256, the in-fan resolution to $\Delta\psi = \pi/768$, which means that r = 3.

Fan data were resorted into semi-parallel groups and then used as the input for the reconstruction. The result of the reconstruction is shown on the left of Fig. 6.

For the simulation of parallel data, the so called WATCH[1] scanning geometry has been realized (see [9] for details). Within this scanning geometry exact parallel data can be acquired either in continuous or in stop-and-start mode. 256 projections with in-projection resolution $\Delta\psi = \pi/768$ were simulated by the same number of photons as for fan data. The reconstructed image is shown in Fig. 6, right.

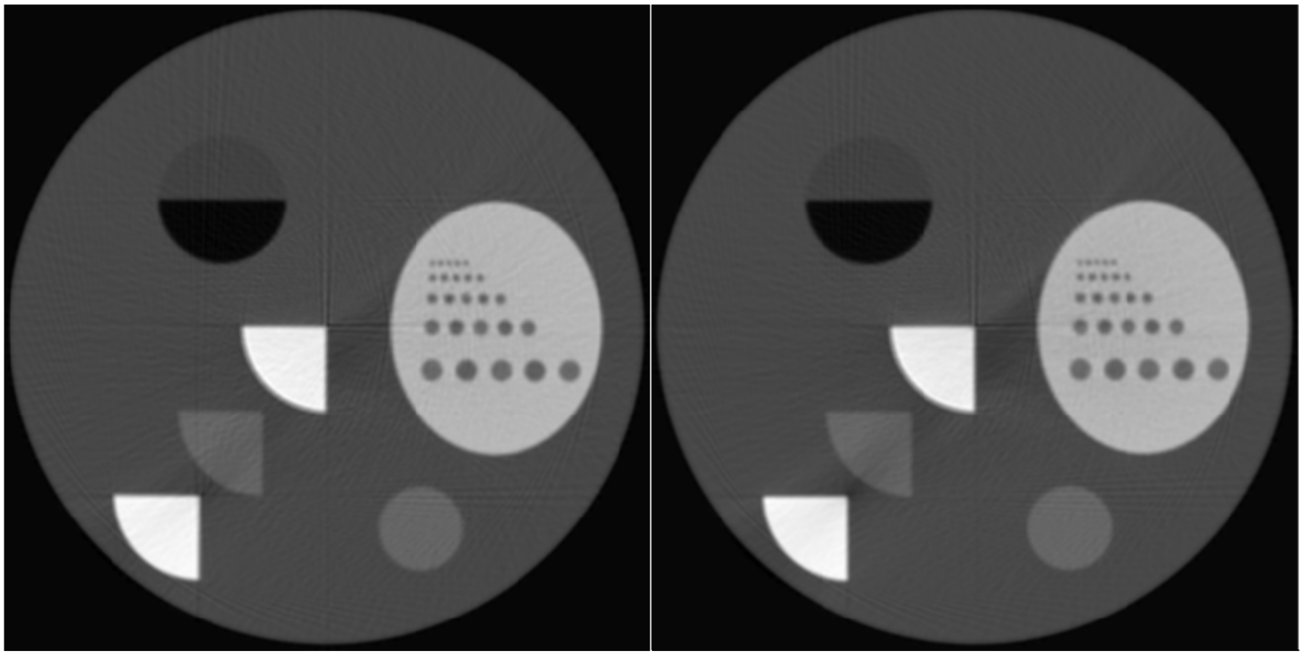

Figure 6. Reconstructions made from fan data (left) and exact parallel data (right). Grid size 512x512, occupied disk area 1/3

The following two examples demonstrate reconstructions from the analytical data of Shepp-Logan phantom calculated by the same value of parameter n, i.e. $n = 256$. This time the data were calculated under the assumption that the phantom occupies a whole disk area. First example, shown in Fig. 7, handles the case $r = 3$. On the top of the figure, full reconstructions from fan and parallel data are shown left and right respectively. Detailed reconstructions of marked patches from them are shown on the bottom of the figure.

[1] Abbr.: Well Advanced Technique for Computer tomography of High resolution

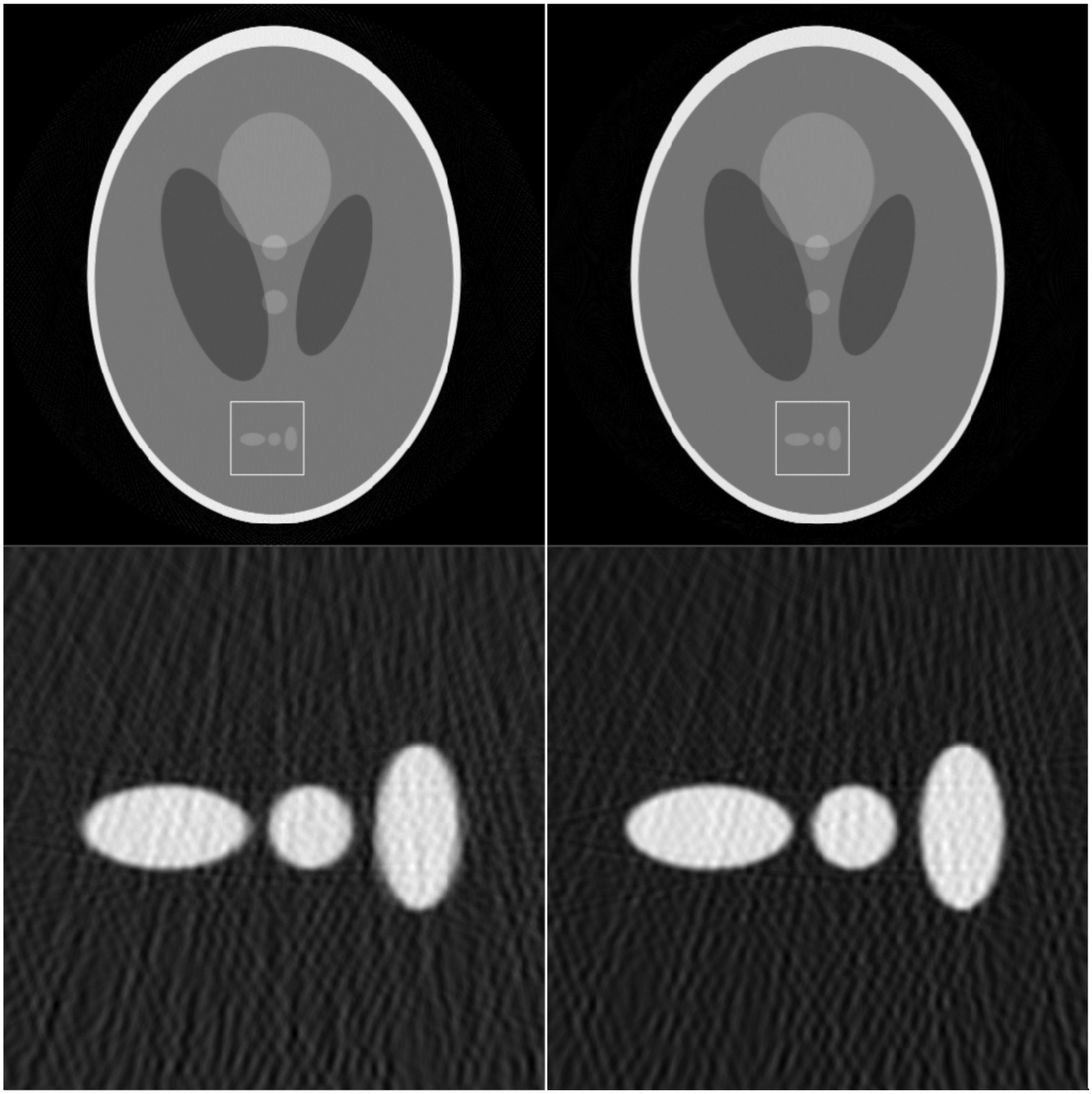

Figure 7. Reconstructions of the analytical Shepp-Logan phantom made by $r = 3$ from fan data (left) and from parallel data (right). Grid resolution 512x512, full disk area

In Fig. 8 the same patches are shown, but this time reconstructions have been made from data calculated for $r = 7$. Full size reconstructions have not a gain on visual quality anymore by the same resolution of the evaluation grid. Therefore they are not shown.

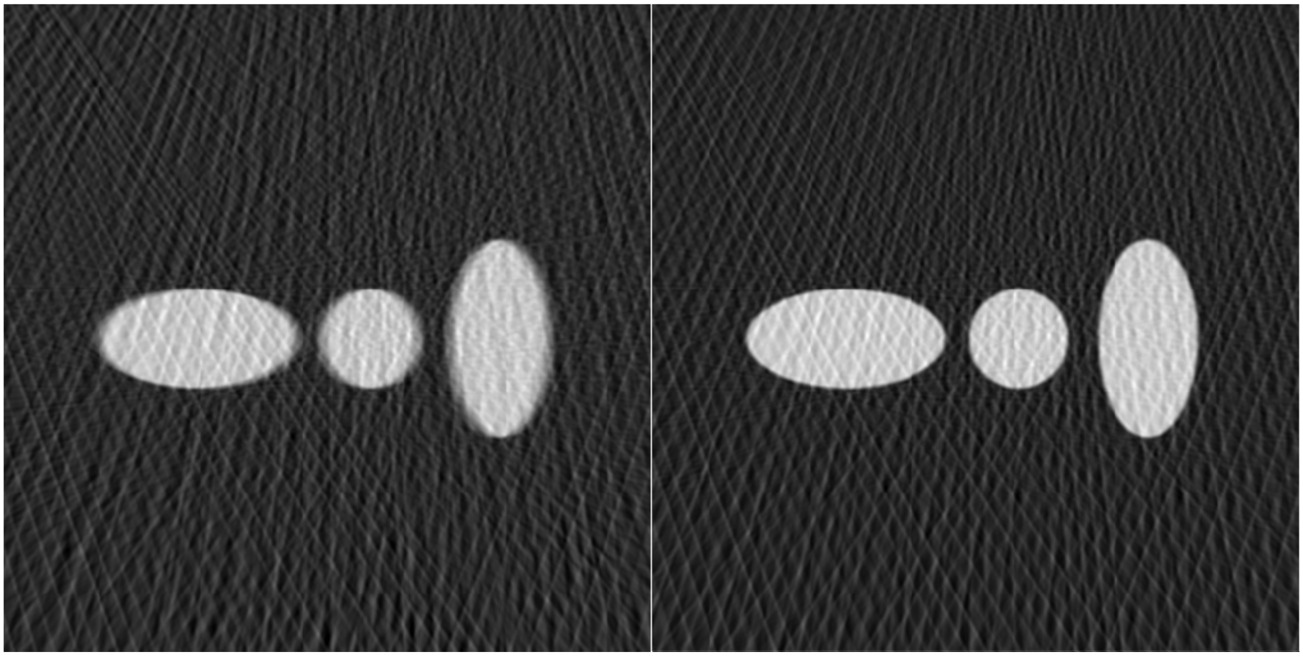

Figure 8. High resolution reconstructions made from fan data (left) and ideal parallel data (right) calculated for $r = 7$

4. DISCUSSION

The described approach of the reconstruction from fan data can be realized with the OPED algorithm. The advantage of the method reveals in that it allows fast reconstructing from fan data. Reconstructed images are very close to images reconstructed from exact ψ-projections. The precision of the reconstruction depends on parameter r introduced in section 2.3.2. If $r = 1$, fan data are equivalent to parallel data of the desired geometry and therefore the method is exact. For $r = 2$ and $r = 3$, deviations of rays from their ideal positions is below $\Delta\psi/2$ and $\Delta\psi$ respectively, where $\Delta\psi$ is in-fan resolution. Such a deviation is quite acceptable, that is, the result of reconstruction is not affected. Note that for modern CT scanners using the third generation geometry $2<r<3$. This follows from the restriction for the scanning geometry using a flying focus technique. This means that the described approach can successfully be applied for the reconstruction of data acquired with scanners of the third generation. For $r > 3$, the deviation of rays of the semi-parallel group is above $\Delta\psi$. However, the method is stable for any r and the quality of reconstruction decreases slowly when r increases and only at fine scales: the difference with the ideal reconstruction, i.e. with the reconstruction made from data collected over rays being at their exact positions, is noticeable at fine scale only. In fact, we expect that this difference decreases when the number of fan views is increased. Thorough study of the quality of reconstruction versus r and number of fan views is the aim of future work.

5. APPENDIX

It has to be shown that

$$\sum_{k=0}^{m-1}(k+1)\sin(k+1)\psi'\sin(k+1)\psi = \frac{m\sin(2m+1)\alpha}{4\sin\alpha} - \frac{\sin^2 m\alpha}{4\sin^2\alpha} - \frac{m\sin(2m+1)\beta}{4\sin\beta} + \frac{\sin^2 m\beta}{4\sin^2\beta} \qquad \text{(A1)}$$

where $\alpha = (\psi - \psi')/2$, $\beta = (\psi + \psi')/2$. The identity

$$\sum_{k=0}^{M-1}(k+1)\sin(k+1)\psi'\sin(k+1)\psi = \sum_{k=0}^{M-1}\sum_{j=k}^{M-1}\sin(j+1)\psi'\sin(j+1)\psi \qquad \text{(A2)}$$

is valid. Substituting well known relations

$$\sum_{k=0}^{m-1} \cos 2(k+1)\alpha = \frac{\sin(2m+1)\alpha}{\sin\alpha} - \frac{1}{2}$$

and

$$\sum_{k=1}^{m-1} \frac{\sin(2k+1)\alpha}{\sin\alpha} = \left(\frac{\sin m\alpha}{\sin\alpha}\right)^2 - 1$$

into (A2) one obtains (A1).

REFERENCES

1. A. Kak, M. Slaney, *Principles of Computerized Tomographic Imaging*, SIAM, Philadelphia, PA, 2001.
2. G. N. Ramachandran, A. V. Lakshminarayanan, “Three-dimensional reconstruction from radiographs and electron micrographs: application of convolutions instead of Fourier transforms”, *Proc. Nat. Acad. Sci.*, USA, **68**, 2236-40 (1971)
3. Y. Xu, “A direct approach to the reconstruction of images from Radon projections”, *Adv. in Applied Math.,* **36**, 388-420 (2006).
4. Y. Xu, O. Tischenko and C. Hoeschen, “A new reconstruction algorithm for Radon data”, *Proc. SPIE*, **6142**, 791-798 (2006).
5. Y. Xu, O. Tischenko, “Fast OPED algorithm for reconstruction of images from Radon data”, *East. J. Approx.* 12, 427-444 (2007)
6. Y. Xu, O. Tischenko, C. Hoeschen, “Fast implementation of the image reconstruction algorithm OPED, *Proc. SPIE*, **7258**, 72585F(2009)
7. M. Abramowitz, I. Stegun, *Handbook of Mathematical Functions with Formulas, Graphs, and Mathematical Tables*, Chapter 22, New York: Dover, 1965
8. O. Tischenko, Y. Xu, C. Hoeschen, Imaging method and device with dual reading scanner, Patent PCT/EP/2007/010281
9. O. Tischenko, M. Klaften, C. Hoeschen, M. A. Hrabe, Scanner device and method for computed tomography imaging, Patent PCT/EP/2009/004063
10. H. G. Heras, O. Tischenko, Y. Xu, C. Hoeschen, “Experimental proof of an idea for a CT-scanner with dose reduction potential”, *Proc. SPIE*, **6913**, 691307 (2008)
11. M. Klaften, A. Schegerer, O. Tischenko, Y. Xu, T. Förster, M. Hrabé de Angelis, C. Hoeschen, „A new design for a micro CT scanner“, Proc. SPIE, **7258** ,72585D (2009)